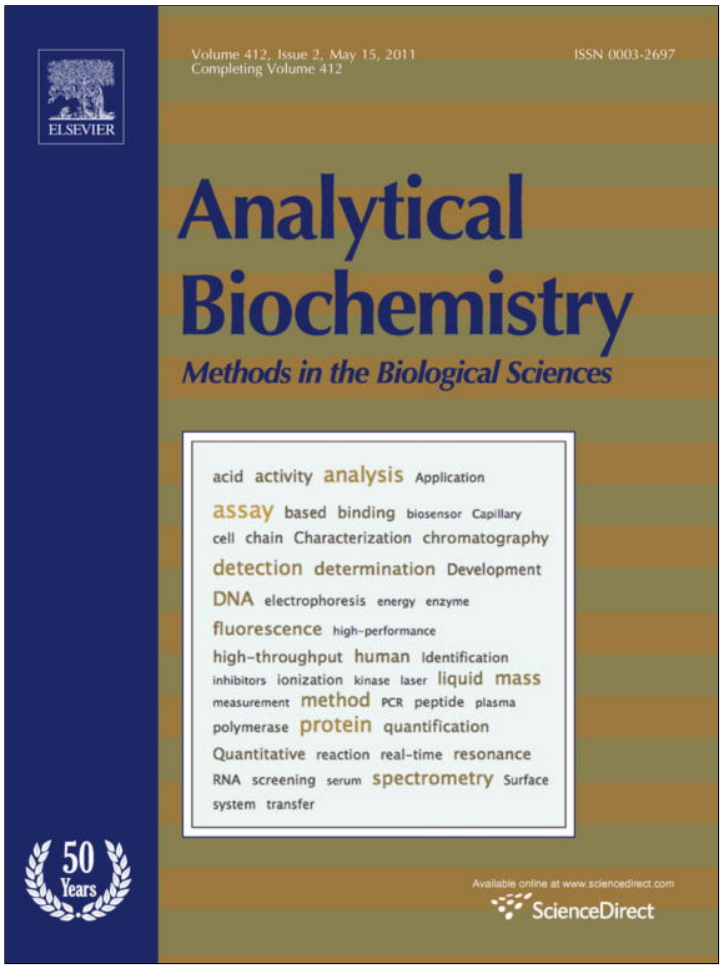

Analytical Biochemistry 412 (2011) 189–202

Contents lists available at ScienceDirect

Analytical Biochemistry

journal homepage: www.elsevier.com/locate/yabio

Limiting the sedimentation coefficient for sedimentation velocity data analysis: Partial boundary modeling and $g(s^*)$ approaches revisited

John S. Philo *

Alliance Protein Laboratories, Thousand Oaks, CA 91360, USA

ARTICLE INFO

Article history:
Received 17 November 2010
Received in revised form 25 January 2011
Accepted 26 January 2011
Available online 1 February 2011

Keywords:
Analytical ultracentrifugation
Direct boundary modeling
Lamm equation
Time derivative analysis
$g(s^*)$ Distribution
Numerical methods

ABSTRACT

Brown and coworkers (Eur. Biophys. J. 38 (2009) 1079–1099) introduced partial boundary modeling (PBM) to simplify sedimentation velocity data analysis by excluding species outside the range of interest (e.g., aggregates, impurities) via restricting the sedimentation coefficient range being fitted. They strongly criticized the alternate approach of fitting $g(s^*)$ distributions using similar range limits, arguing that (i) it produces "nonoptimal fits in the original data space" and (ii) the $g(s^*)$ data transformations lead to gross underestimates of the parameter confidence intervals. It is shown here that neither of those criticisms is valid. These two approaches are not truly fitting the same data or in equivalent ways; thus, they should not actually give the same best-fit parameters. The confidence limits for $g(s^*)$ fits derived using F statistics, bootstrap, or a new Monte Carlo algorithm are in good agreement and show no evidence for significant statistical distortion. Here 15 $g(s^*)$ measurements on monoclonal antibody samples gave monomer mass estimates with experimental standard deviations of less than 1%, close to the confidence limit estimates. Tests on both real and simulated data help to clarify the strengths and drawbacks of both approaches. New algorithms for computing $g(s^*)$ and a scan-differencing approach for PBM are introduced.

Sedimentation velocity experiments can be quite useful for measuring solution molar mass to identify the state of oligomerization of single proteins or the stoichiometry of multiprotein complexes. In practice, however, protein samples often contain minor components in addition to the species of interest such as irreversible aggregates, protein impurities, or "incompetent monomers" (improperly folded monomers that do not assemble in the normal fashion). Although sophisticated data analysis methods now exist that can model samples containing multiple components, and that require no assumptions about how many components are present, they have certain drawbacks. For example, the $c(s)$ method [1] is relatively robust and quick to compute, but the minor components will affect the weight-average frictional coefficient ratio f/f_0 that best fits the whole sample; therefore, they will influence the apparent molar mass of the main component. Two-dimensional distribution methods such as $c(s, f/f_0)$ [2] and two-dimensional spectral analysis (2DSA)[1] [3] remove that drawback but are computationally quite intensive.

Thus, for answering important but relatively simple questions such as "Is the native state of my protein really a tetramer?" it is desirable to have a simple and rapid data analysis method that focuses on the major component and avoids explicitly modeling and characterizing the minor species that are not of interest. One way to do this is to limit the range of sedimentation coefficients being considered in the fitting so that only the major component needs to be modeled, and there are now two distinct approaches to achieve this. One approach is to first transform the raw velocity scans into the $g(s^*)$ distribution via time-derivative methods [4], set the desired fitting range to exclude the high and/or low sedimentation coefficient regions of the distribution (leaving the main peak), and then fit this portion of the $g(s^*)$ distribution [5,6] as a single component. Recently, Brown and coworkers [7] developed an alternative approach where the sedimentation coefficient range limits are imposed by fitting only a limited radial range of each scan (a range that moves outward along with the boundary in successive scans). This limited portion of the boundary is then fitted by direct boundary modeling. They referred to this approach as partial boundary modeling (PBM).

The PBM approach, in principle, allows including all of the scans in the analysis and allows fitting the meniscus position, which the $g(s^*)$ approach does not allow. Although it was argued by Brown and coworkers that these constitute important advantages [7], they did not directly test whether these properties significantly

* Fax: +1 805 388 7252.
E-mail address: jphilo@mailway.com

[1] *Abbreviations used:* 2DSA, two-dimensional spectral analysis; PBM, partial boundary modeling; TIN, time-independent noise; TRAP, *trp* RNA-binding attenuation protein; BSA, bovine serum albumin; SV, sedimentation velocity; OD, optical density; RMSD, root mean square deviation; RIN, radially independent noise.

0003-2697/$ - see front matter © 2011 Elsevier Inc. All rights reserved.
doi:10.1016/j.ab.2011.01.035

improve the accuracy or precision of the results. Furthermore, that work strongly criticized the $g(s^*)$ fitting approach, stating that (i) the data transformations used in calculating $g(s^*)$ strongly distort the statistical properties of the fits and lead to gross underestimates of the parameter confidence intervals, (ii) the results are highly sensitive to minor differences in the scan subset used in the analysis and other analyst choices, and (iii) it produces "nonoptimal fits in the original data space," implying that the results have been significantly distorted by the $g(s^*)$ transformation. These claims call into question the results from many of the more than 200 published studies that have used $g(s^*)$ analysis. However, none of these claims appears to have been tested based on adequate controls or by using data where the correct answers are known.

Therefore, one major goal of the current investigation was to reexamine these issues and clarify the differences between the PBM and $g(s^*)$ methodologies. As one part of that effort, a new algorithm that allows Monte Carlo methods to be applied to $g(s^*)$ fitting was developed. Results obtained from fits to simulations as well as new experimental studies do not validate the existence of the $g(s^*)$ fitting problems proposed in Ref. [7]. Furthermore, in the course of comparing these two software approaches, some significant statistical issues arising with the PBM method were uncovered, and these new results also are inconsistent with some of the key advantages claimed for the PBM method.

One significant drawback of calculating $g(s^*)$ via the time-derivative method [4,8] has always been the need to use only a relatively small fraction of the scans (a limited range of boundary movement) to avoid artificial broadening of the peaks in the $g(s^*)$ distribution (loss of resolution). This is an important issue for this context of trying to eliminate the influence of minor components based on their sedimentation coefficients, but it appears that there is some confusion [7] about whether the "improved" $g(s^*)$ fitting algorithm [9] is intended or able to eliminate this drawback. Furthermore, the major cause of this peak broadening effect has not previously been discussed explicitly [4,6,8,9], and it is also highly relevant to whether PBM and $g(s^*)$ fits can be directly compared. Therefore, a second aim of this study was to clarify the origin and significance of the peak broadening and to introduce a new modification to the time-derivative algorithm that can reduce the broadening and allow a broader range of scans to be used.

These studies indicate that the normal procedure in PBM analysis of removing the baseline variation across the cell by fitting the time-independent noise (TIN) rather than by scan differencing, as is done in $g(s^*)$ analysis, is a major source of the differences between these approaches and a major reason why the precision of the mass estimates from PBM analysis appears to often be lower than that from $g(s^*)$ fitting. Therefore, a new algorithm that allows scan differencing to be used with PBM is also introduced and briefly compared with conventional PBM using a fitted TIN.

It should be noted that the PBM, $g(s^*)$, $c(s)$, $c(s, f/f_0)$, and 2DSA analysis methods mentioned above all are treating reversible oligomers or complexes as a single independent species rather than explicitly treating the reversible dissociation into monomers or subunits. Such treatment is reasonable, and has been shown to give the correct molar mass and stoichiometry, when the protein concentration is high enough that no significant dissociation occurs. Some examples where $g(s^*)$ analysis has been used to determine stoichiometry of reversible oligomers, with verification from sedimentation equilibrium or other orthogonal approaches, can be found in Refs. [10–14]. However, exactly what concentration is high enough for this purpose has not, to our knowledge, been discussed previously, so a limited exploration of this issue is made here. But clearly, at protein concentrations where there is substantial interconversion of species during the separation, approximating a reversible complex as a single species will not be valid, and in such cases the association equilibria must be explicitly modeled.

Materials and methods

The PBM fits were done using SEDPHAT version 6.5 [7]. The $g(s^*)$ analyses were done using DCDT+ version 2.2.3 [9]. The whole boundary fits using the new multisection algorithm for scan differencing and with PBM restrictions on the sedimentation coefficient range were done using SVEDBERG version 7.0 [15]. The *trp* RNA-binding attenuation protein (TRAP) and bovine serum albumin (BSA) simulations were created using SEDFIT version 11.3 [1].

The sedimentation velocity experiments on the monoclonal antibody samples were run at 0.5 mg/ml and 35,000 rpm using absorbance scans acquired every 4 min. The meniscus position was fixed at the top of the meniscus spike (the mean of that position for all of the scans in the run). The $g(s^*)$ distributions were calculated using a subset of 16 scans starting at whatever time point gave a distribution extending out to approximately 12 S. Those distributions were then fitted as a single species with the sedimentation coefficient range restricted to the central portion (between the 50% amplitude points) of the main (monomer) peak.

Results and discussion

Do the g(s) data transformations cause significant underestimates of the parameter uncertainties?*

Brown and coworkers [7] asserted that the data transformations used in generating $g(s^*)$ distributions cause serious distortions of the fit statistics and lead to significant underestimates of the parameter uncertainties. That conclusion was based in part on their analyses of an sedimentation velocity (SV) data set for TRAP complexes. TRAP has been shown to form 11-mer complexes (91.6 kDa) [16,17]. This TRAP data set had previously been used to illustrate an improved algorithm for fitting $g(s^*)$ distributions [9]. The authors found that the confidence interval estimated for their PBM fit of the TRAP experimental data using 12 scans starting at scan 23 gave 95% confidence limits approximately 2-fold wider than those reported previously for the corresponding $g(s^*)$ fit using those same scans [9]. In addition, they concluded from their PBM analysis using all 67 scans that this data set can determine the mass of the main component only within ±2.4 monomer units at 95% confidence and, therefore, assumed that the ±0.4 monomer units confidence interval from $g(s^*)$ fitting of only 12 scans must be a gross underestimate. However, these PBM and $g(s^*)$ fits are really not equivalent, and it is shown later that the confidence limits from these two approaches are significantly different (both were reported correctly).

Error surfaces for the TRAP experiment and simulation

Fig. 1A shows error surfaces for the mass parameter resulting from fits of the TRAP data set. This protein reportedly primarily forms 11-mer complexes [17], but this particular sample was not of high quality (it was run at a workshop demonstration) and also contains aggregates. The solid green curve shows results for a PBM fit of all 67 scans as a single species using sedimentation coefficient fitting limits of 4.39 to 6.28 S, which essentially reproduces Fig. 4d from Ref. [7]. These results, as reported, indicate that by PBM the best-fit stoichiometry is approximately 9.7 subunits and the 95% confidence interval includes any stoichiometry between approximately 7.3 and 12.4 subunits. However, the error surface from the $g(s^*)$ fit using only 12 scans starting with scan 23 (dashed blue curve) [9] is much more strongly curved (much more sensitive to changes in the best-fit mass). Although it would not be correct to apply the same critical χ^2 limits used for the PBM fit (horizontal green lines) to the $g(s^*)$ fit because the degrees of freedom are not the same, it is quite clear that the error surfaces are

qualitatively different and that the $g(s^*)$ fit appears to be much more sensitive to the mass value and, thus, should have a lower confidence limit.

But why is the PBM fit less able to define a unique mass even though it uses many more scans, the opposite of what we might expect? One important reason why the PBM error surface is broad is that this is one consequence of removing the baseline variation across the cell via fitting the TIN,[2] which introduces hundreds of additional fitting parameters into the analysis (up to ~1600 parameters for interference scans). Because the computed TIN directly depends on the hydrodynamic parameters, the TIN changes as the mass is varied to construct the error surface, and those changes in TIN substantially reduce the increase in χ^2 that would otherwise occur. This is demonstrated by the red dotted curve in Fig. 1A, which was computed by holding the TIN fixed at the best-fit value while the mass was varied.[3] This comparison shows that fitting the TIN roughly doubles the width of the confidence interval. Note that it is *not* being argued that holding the TIN fixed is the proper way to evaluate the confidence interval for the PBM fit; the purpose of this exercise was to try to parse out the effects of the differing approaches to removing systematic noise. Note that broader confidence intervals when the TIN is fitted were also observed in the original report of this TIN removal algorithm [19].

Although fitting the TIN clearly is one important reason why the error surfaces for the PBM and $g(s^*)$ surfaces are very different, is the $g(s^*)$ result truly underestimating the parameter uncertainty and, if so, is that a general property or something specific to this experiment? An important difficulty with real experiments is that we do not know the true properties of the sample or even whether the noise in the raw data is actually random. Therefore, these questions are best addressed using simulated data where the noise levels and the correct parameter values are known. Thus, this TRAP experiment was simulated as a mixture of 11-mer plus 22-mer, 33-mer, and 44-mer in the proportions and at the sedimentation coefficients obtained using the SEDPHAT hybrid-discrete model in Ref. [9]. The random noise of 0.00358 optical density (OD) added to these simulations corresponds to the root mean square deviation (RMSD) reported in Ref. [7] for the PBM fit of scans 23–32, the scans used for the original $g(s^*)$ fit in Ref. [9].

Fig. 1B shows error surfaces from fits of this TRAP simulation corresponding to those from the experimental data in Fig. 1A. These results show that the relative shift of the best-fit mass between the $g(s^*)$ and PBM results in Fig. 1A is indeed a specific feature of that data set, but the major difference in the curvature of the error surfaces is not. The horizontal lines indicate the critical χ^2 levels corresponding to 68.3 and 95% confidence levels for the PBM and $g(s^*)$ fits. Those critical values are, of course, higher for the $g(s^*)$ fit because the number of data points being fitted is lower,[4] but nonetheless the confidence limits for the $g(s^*)$ fit are considerably narrower than those for the PBM fit (±0.38 vs. ±1.61 subunits at 95% confidence).[5]

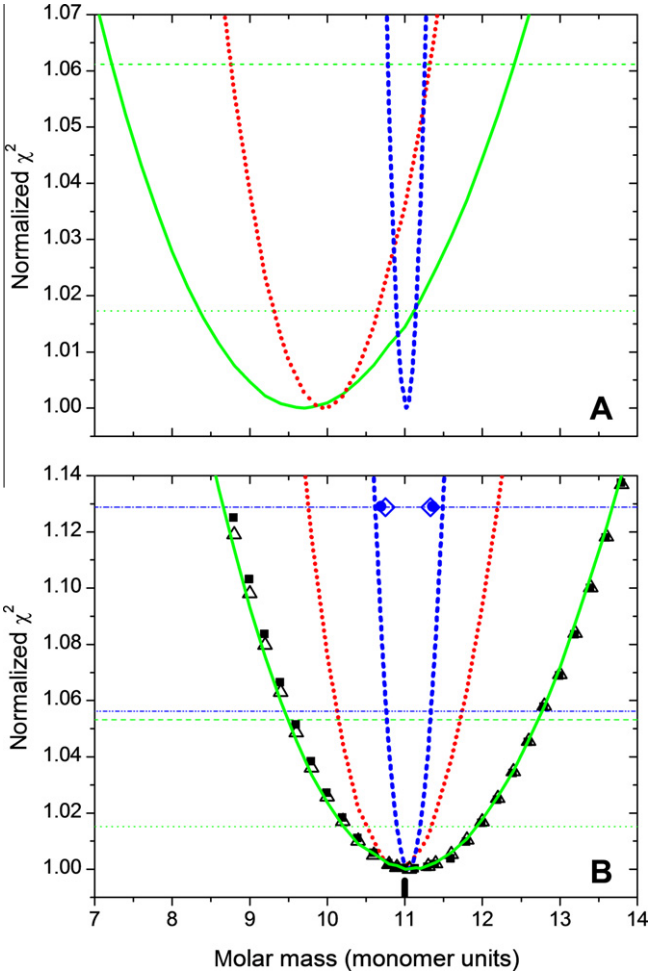

Fig.1. Changes in fit quality versus molar mass for fits of the TRAP experimental data (A) and simulations of that experiment (B). The ratio of the χ^2 observed for each mass was divided by the value observed for the best fit to give the normalized χ^2 value. For each type of fit, the molar mass was fixed at various values over the range shown, whereas the remaining parameters were reoptimized. The green solid curves are for PBM fits using all 67 scans with sedimentation coefficient limits of 4.39 to 6.28 S, and the horizontal dotted and dashed green lines indicate the critical χ^2 values corresponding to the 68.3 and 95% confidence levels, respectively, calculated by SEDPHAT. The red dotted curves give the results for this PBM fit if the TIN is held fixed at the values from the best fit rather than being reoptimized as the molar mass is varied. The blue dashed curves show the results from fitting the $g(s^*)$ distribution derived from scans 23 to 32 of the real data with sedimentation coefficient limits of 4.39 to 6.28 S and a corresponding fit of the simulation. In panel B, the thick vertical black line indicates the correct mass (the value used in the simulation) and the blue horizontal dash-dot and dash-dot-dot lines show the critical χ^2 values at the 68.3 and 95% confidence levels calculated by DCDT+. The blue open diamonds and blue solid circles show the 95% confidence limits for the $g(s^*)$ fit calculated using the bootstrap and Monte Carlo methods, respectively. The open black triangles show the error surface for the PBM analysis when the first 28 scans are omitted from the fit, and the filled black squares give the results for that fit when the meniscus is held fixed at the known value. (For interpretation of the references to color in this figure legend and the text, the reader is referred to the Web version of this article.)

New bootstrap and Monte Carlo estimates of parameter uncertainties for g(s) fits*

A major drawback to estimating confidence intervals using *F* statistics is that this requires assumptions about the statistical properties of the data. The bootstrap method with replacement [20] is an alternative approach for estimating confidence intervals that avoids those statistical assumptions, and it has now been implemented for $g(s^*)$ fits. In this approach, a new data set is created by randomly choosing data points from the fitted region of the $g(s^*)$ distribution. This new data set has the same total number

[2] The calculation of the TIN should properly be described as "fitting" the TIN. Although it is true that separation of linear and nonlinear parameters [18] allows the TIN to be calculated algebraically during each iteration of the fit, the elements of the TIN vector are still fitting parameters and are not independent of the values of the other fitting parameters.

[3] The best-fit TIN was subtracted from each scan, and the resultant data were fitted without TIN or offset.

[4] Note that the number of data points in a $g(s^*)$ distribution depends on the increment of sedimentation coefficient between successive points. In DCDT+, this increment is chosen such that the number of points in the distribution approximately matches the number of data points in the region of a raw scan that is used in calculating $g(s^*)$.

[5] Confidence limits as calculated by DCDT+ are not assumed to be symmetric around the best-fit value, but to allow easier comparison with those calculated by SEDPHAT, the difference between the upper and lower limits reported by DCDT+ has been divided by 2 to give the equivalent "±" range.

of data points as the original set, but the random selection means that some points from the original distribution will be selected more than once and others will not be selected at all (hence "with replacement"). This new data set is fitted, and this whole process is then repeated many times to create a table of best-fit parameter values. Finally, the observed standard deviation of the tabulated parameter values from the bootstrap is used to estimate the confidence limits. Applying the bootstrap method to the $g(s^*)$ fit of the TRAP simulation (2000 rounds) gives 95% confidence limits of 10.75–11.33 monomer units, as shown by the blue open diamonds in Fig. 1B. That is, this approach gives a somewhat narrower confidence region than that from *F* statistics.

The bootstrap method, however, operates in the $g(s^*)$ data space and, therefore, cannot directly address whether the $g(s^*)$ transform itself is distorting the raw data in a way that leads to a significant underestimate of the confidence interval, as hypothesized by Brown and coworkers [7]. Therefore, a new approach that allows Monte Carlo methods to be applied to $g(s^*)$ fitting has been implemented. The "improved algorithm" for fitting the $g(s^*)$ distributions [9] always generates noise-free theoretical boundaries corresponding to each raw scan (but without the TIN); thus, random noise can be readily added to those noise-free boundaries to generate theoretical $g(s^*)$ distributions where the noise was random prior to the transformation. However, the standard Monte Carlo approach cannot be applied here because the residuals from the $g(s^*)$ fit do not provide a direct and accurate measure of the noise level of the original raw data. For fits of simulated data, this is not an issue because the true noise level of the simulated raw scans is known. For real experiments, it is possible to set the correct noise level for the Monte Carlo simulations through the following iterative procedure: (i) the noise in the raw data is estimated from the RMSD of the fit to $g(s^*)$ by assuming that the noise in $g(s^*)$ varies inversely with the sedimentation coefficient (the expected pattern if the noise in the raw data is random); (ii) the estimated noise level is used for *n* rounds of Monte Carlo simulations and fits and then the mean RMSD in $g(s^*)$ from those Monte Carlo fits is compared with the RMSD of the experimental fit; (iii) if the mean RMSD of the Monte Carlo rounds is too far off from the experimental RMSD, the random noise for the simulations is scaled up or down based on the ratio of the Monte Carlo to experimental RSMD values and the algorithm returns to the second step (ii). This iterative process is simply continued until the Monte Carlo RMSD matches the experimental one within some desired precision. Two or three iterations is usually sufficient for a match within a few percentage points, and for this TRAP fit an iteration with 500 Monte Carlo rounds requires only approximately 30 s on a modern processor.

When this modified Monte Carlo algorithm is applied to the TRAP simulation (using the known noise level of that simulation) the result from 2000 rounds is 95% confidence limits for the mass of 10.70–11.37 subunits (solid blue circles in Fig. 1B). Thus, these values fall in between those from bootstrap or *F* statistics. Similarly, the Monte Carlo runs for the corresponding fit of the real experiment give 95% confidence limits of 10.67–11.36 subunits, entirely consistent with the 10.7–11.4 limits that were originally reported based on *F* statistics [9]. This proves that the $g(s^*)$ transformation is *not* causing significant underestimates of the confidence intervals for this experiment. Moreover, this Monte Carlo analysis proves that the $g(s^*)$ distribution derived from only 12 scans does contain more than sufficient information to define the stoichiometry (to determine the mass with precision better than ±0.5 subunit) at 95% confidence. It is also important to note that the confidence limit estimates based on the statistical properties of the transformed data (by *F* statistics or the bootstrap method) are actually in remarkably good agreement with each other and the Monte Carlo results considering that they derive from quite different statistical approaches.

Is the lower parameter precision (larger confidence interval) of the PBM fits of the real and simulated data a general result or unique to some feature of this TRAP experiment? To explore that issue, a simulation was also done of the BSA experiment described by Brown and coworkers [7]. The details of the minor component content of that sample were not reported, but commercial BSA preparations typically contain approximately 15% aggregates. Therefore, this simulation assumed a BSA dimer content of 12% and a trimer content of 3%, and this does give $g(s^*)$ and $c(s)$ distributions similar to those shown in Fig. 5 in Ref. [7]. PBM fits of this simulation as a single species were done using scans 10 to 69 (matching the maximum scan range used in Ref. [7]) and with a fitting range of 3.70–5.80 S (corresponding to the peak half-height of the $g(s^*)$ main peak at the time the monomer has reached the middle of the cell). However, such fits were not successful if the meniscus position was fitted. Fit attempts using either the simplex or simulated annealing fitting algorithms resulted in "invalid geometry or s, D parameters" errors. With the Marquardt–Levenberg algorithm, no error messages occurred, but there was no true convergence; a best-fit mass within a few hundred Daltons of the initial guess was returned for any initial guess between 32 and 82 kDa. By fixing the meniscus at the known position, it was possible to get reproducible convergence when using the simulated annealing option, and that fit returns a best-fit mass of 67.68 kDa (2.0% above the true value). Fig. 2A shows the error surface from that fit (solid green line), which gives a 95% confidence interval for the monomer mass of 57.9–78.1 kDa (−12.7% to +17.6% from the correct value). Thus, although the PBM fit appears to give a fairly accurate result (it is not biased significantly away from the correct value), it is a result with rather low precision. For comparison, a $g(s^*)$ analysis using only 14 scans (37–50) and fitting the central half of the main peak returns 65.89 kDa (−0.7%) with a 5-fold narrower Monte Carlo 95% confidence interval of 63.79–67.80 kDa (−3.9% to +2.1%).

Once again, it appears that the broad error surface (low precision) of the PBM fit is largely a consequence of the strong variation of the fitted TIN as the monomer mass value changes. Fig. 2B shows some of the simulated scans (every third scan) and the actual regions that were fitted. The heavy blue solid and green dashed lines in Fig. 2B show the TIN values from fits with the mass held at either the upper or lower 95% confidence limit. Both of these TIN curves are significantly shifted away from zero (the correct value) at all radii; the green curve is nearly constant at approximately −0.0037 OD across the entire radial range, whereas the blue one falls from approximately 0.005 OD near 6.1 cm to 0.0035 OD at 7.1 cm. These physically unrealistic TIN values allow the best-fit concentration for the BSA monomer to deviate significantly from the true value without a substantial increase in RMSD, which largely compensates for the nonoptimal mass. When the mass is at the lower 95% confidence limit, the best-fit monomer concentration is 5.3% higher than the true value; when the mass is at the upper limit, the best-fit monomer concentration is 4.7% lower than the true value.

Experimental test of mass precision

To further test whether fitting the $g(s^*)$ distribution produces significant underestimates of the parameter uncertainties, mass estimates for the main component (monomer) were made from 15 data sets for a monoclonal antibody by fitting only the central half of the main $g(s^*)$ peak (between the 50% height points). These 15 data sets cover five different manufacturing lots, each measured in triplicate, which by $c(s)$ analysis contain approximately 1–3% total aggregates and 0.5% antibody fragments. The correct partial specific volume for this antibody and the solvent density are not known, so the buoyant mass rather than the molar mass was computed, and those values are summarized in Fig. 3. The mean of the

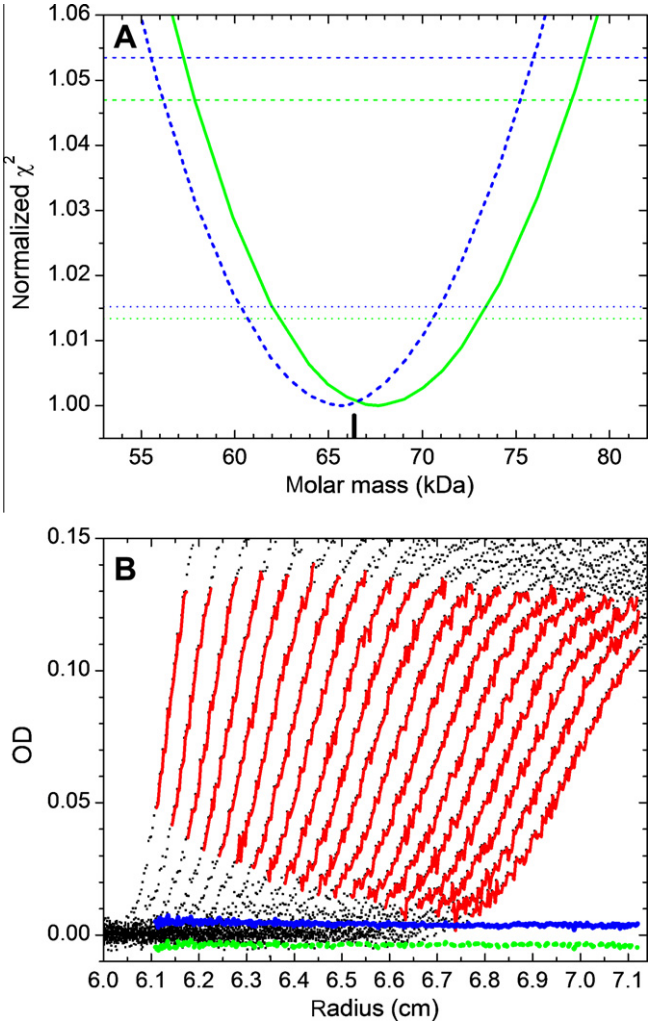

Fig.2. (A) Changes in fit quality (normalized χ^2 values) versus molar mass for a PBM fit (range of 3.70–5.80 S) as a single species with a fitted TIN for scans 10 to 69 of a simulation of the BSA experiment at 50,000 rpm described by Brown and coworkers [7]. The BSA sample was assumed to contain 85% monomer at 66.376 kDa and 4.58 S, 12% BSA dimer at 6.93 S, and 3% trimer at 8.52 S. The loading concentration was 0.20 OD, the added root mean square noise was 0.002 OD, and scans were recorded every 3 min. The thick vertical black line indicates the correct mass (66.376 kDa, the value used in the simulation). The dashed blue curve gives the error surface for a similar fit but using only scans 34 to 69. The horizontal dotted and dashed blue and green lines indicate critical χ^2 values corresponding to the 68.3 and 95% confidence levels (as calculated by SEDPHAT) for the blue and green curves. (B) Simulated scans (black points) and their portions included in the PBM fit (red lines). Scan 10 and every third scan thereafter are shown. Also shown as heavy green dashed and blue solid lines are the TIN profiles resulting from fits with the mass held at the lower and upper 95% confidence limits, respectively. (For interpretation of the references to color in this figure legend and the text, the reader is referred to the Web version of this article.)

15 mass estimates is 38.84 kDa with an experimental standard deviation of ±0.34 kDa (a relative standard deviation of only 0.88%), which implies a 95% confidence interval of ±0.67 kDa (the dashed red lines in Fig. 3). It is hardly surprising that this experimental confidence interval is somewhat larger than the ±0.42 kDa estimated by the Monte Carlo simulations (the mean of the 15 Monte Carlo estimates, 500 rounds each, shown as the blue dotted lines). The mean confidence intervals from *F* statistics of ±0.44 kDa, and from the bootstrap method (500 rounds) of ±0.52 kDa, are quite consistent with the Monte Carlo estimate but again are also somewhat lower than the experimental value. The key point is that the experimental confidence limit is actually only approximately 30–60% larger than the statistical estimates

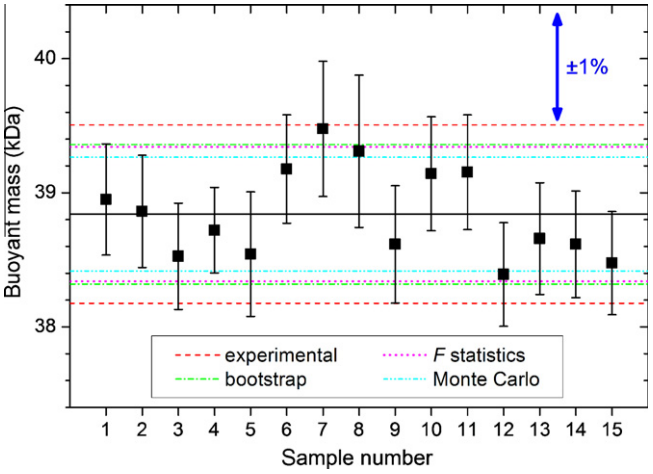

Fig.3. Estimated buoyant masses (black squares) from fitting the central half of the main $g(s^*)$ peak for 15 samples of a monoclonal antibody (five different manufacturing lots, each measured in triplicate). The error bars on each point show the 95% confidence limits from each fit estimated via Monte Carlo simulations (500 rounds). The solid black horizontal line is the mean of the 15 measurements. The dashed red lines show the experimental 95% confidence limits (based on the actual standard deviation of the 15 observations). The dotted magenta, dash-dot green, and dash-dot-dot cyan lines show estimated 95% confidence limits based on the mean of the 15 confidence intervals computed via *F* statistics, bootstrap, and Monte Carlo analysis, respectively. (For interpretation of the references to color in this figure legend and the text, the reader is referred to the Web version of this article.)

despite the fact that real experiments clearly will have significant sources of error other than random photometric noise. Thus, these real experiments do *not* support a conclusion that either the $g(s^*)$ transformation itself or the specific choices of scan subsets or meniscus position are significantly distorting the estimated parameter precision, as was argued by Brown and coworkers [7]. These data also demonstrate that this approach gives precise and reproducible results.

Variability of hydrodynamic parameters with scan selection, sedimentation coefficient limits, or meniscus position

From their own $g(s^*)$ analyses of the TRAP experiment, Brown and coworkers [7] correctly observed that the apparent stoichiometry of the TRAP complex can vary significantly as a function of analyst choices such as the subset of scans used in computing the $g(s^*)$ distribution and with simultaneous changes in the range of sedimentation coefficients included in the fitting and the position of the meniscus. However, not all of those changes are unexpected or indicative of problems with this method. Furthermore, their study did not include controls to distinguish which effects are related to specific data analysis methods or analyst choices and which are peculiarities of this specific experiment. To distinguish which of these effects are inherent to a data analysis method and which might be specific to this particular experiment, it is essential to use data where the correct answers are known.

Fig. 4A summarizes results for many different $g(s^*)$ fits of the TRAP data using different selections for the subset of scans (earlier or later in the run and using 8, 12, or 16 total scans) and with variations in meniscus position and the sedimentation coefficient range. These analyses essentially reproduce Fig. 3b in Ref. [7], whereas Fig. 4B shows the same fits but using the simulated data. A systematic drop in apparent mass does occur when the analysis uses scans early in the run, but this is actually expected. The aggregates in the sample are simply not resolved from the main component early in the run; therefore, limiting the range of sedimentation coefficients being fitted cannot fully exclude the aggregate influence on the

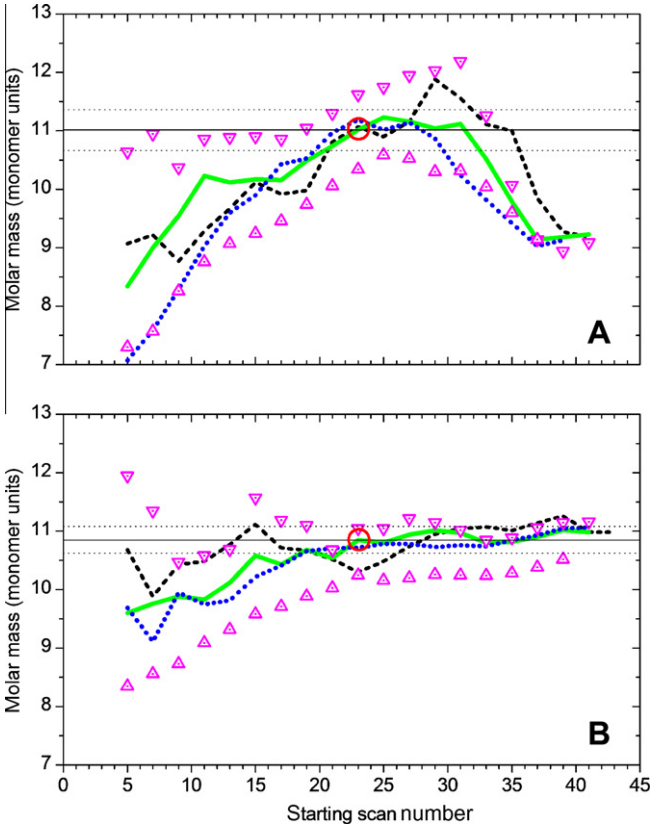

Fig.4. Dependence of the apparent molar mass from $g(s^*)$ fits of the TRAP experiment (A) and simulation (B) with fitting limits of 4.39 to 6.28 S when using different subsets of scans, starting with the scan number indicated on the abscissa, for a total of 8 scans (dashed black curve), 12 scans (solid green curve), and 16 scans (dotted blue curve). Also shown are the results for groups of 12 scans with a shift of the assumed meniscus position by –0.01 cm and a narrower fitting range from 4.65 to 6.03 S (downward-pointing triangles) and with the meniscus shifted by +0.01 cm and a wider fitting range from 4.03 to 6.91 S (upward-pointing triangles). The red circle marks the conditions for the "default" fit using 12 scans starting at scan 23. The thin black horizontal line indicates the mass from that fit, and the dashed horizontal black lines are the 95% confidence limits for that fit obtained via 500 rounds of Monte Carlo simulation. (For interpretation of the references to color in this figure legend and the text, the reader is referred to the Web version of this article.)

results (see Fig. S1 in supplementary material). That is, the model being fitted is inherently incorrect for the early scans, and if the data analysis is properly sensitive to heterogeneity in the sample, the inclusion of early scans *should* produce a mass estimate lower than the true mass of the main component. A comparison of Fig. 4A and B, however, shows that the mass drop when using early scans is significantly larger for the real experiment than with the simulated data, so it appears that some additional factor is influencing this particular experiment.

For the real experiment, the significant drop in apparent mass for fits using scans late in the run (starting after ~ scan 30) is an unexpected feature. This pattern is totally absent in Fig. 4B, so clearly this too represents a specific feature of this experiment. These differences between the experiment and simulation might indicate that this sample was not behaving as a simple mixture, perhaps due to dynamic redistribution between different types of complexes. Note also that the differences between results obtained using 8, 12, and 16 total scans (black, green, and blue solid lines, respectively) are significantly smaller for the simulation than in the actual experiment.

Probably the most important point, however, is that the simulation fits show that the stoichiometry is correctly determined by $g(s^*)$ fitting over a fairly wide range of scan subset and other analysis choices. The simulation further clarifies that the "default" fit starting with scan 23 uses scans only barely late enough in the run for adequate resolution of the aggregates from the main peak. Nonetheless, the correct stoichiometry is obtained for all of the fits that use the default sedimentation coefficient limits and 12 or 16 scans starting at scan 19 or later. The stoichiometry is also correct for all but one of those fits using only 8 scans (with only 8 scans, the signal/noise ratio is insufficient to reliably define the stoichiometry within ±0.5 subunit). The use of a narrower sedimentation coefficient range together with a meniscus position shift of −0.01 cm (downward-pointing triangles) still gives the correct stoichiometry for all analyses starting at scan 11 or later. The use of a much broader sedimentation coefficient range (4.03–6.91 S) together with a meniscus shift of +0.01 cm (upward-pointing triangles) does, however, give an incorrect stoichiometry (too low) in nearly every case. However, that occurs because the upper limit of 6.91 S does not sufficiently exclude the influence of the aggregates (the simulated 22-mer is at 7.48 S). That is, these fits are correctly sensing that a single species is not sufficient to explain the range of data that are being fitted, and the residuals do show systematic deviations for sedimentation coefficients $\geqslant$6.4 S.

Brown and coworkers [7] concluded from their analysis of the TRAP data that the mass returned by the $g(s^*)$ fits has "a strong dependence on small changes in meniscus." This conclusion, however, was not based on adequate controls. In the analyses shown in their Fig. 3b, changes in the assumed meniscus position were always coupled with simultaneous changes in the sedimentation coefficient range being fitted, making it impossible to distinguish the true influence of the meniscus position. Furthermore, because the assumed meniscus position affects the apparent sedimentation coefficients of all species, a controlled test of the meniscus effect requires shifting the fitting range to keep it in the same position relative to the main component's peak in the $g(s^*)$ distribution; otherwise, the minor components will shift in or out of the fitting range as the meniscus position is changed. With this controlled approach, the apparent masses from the fits of the TRAP simulation change by only ± 1% for changes of the assumed meniscus position of ±0.005 cm (a region larger than the entire width of the meniscus region in a typical absorbance scan). Thus, the meniscus uncertainty has a minimal effect on the mass precision in real applications of this approach (probably much smaller than the effect of uncertainty in the correct partial specific volume).

In summary, reproducible results giving the correct stoichiometry can be obtained through the $g(s^*)$ approach over a fairly wide range of data subsets and other analyst choices provided that the analyst avoids (i) including the scans where the aggregates are not yet separated from the main peak and (ii) choosing a sedimentation coefficient range such that the aggregate contributions are not excluded. That is, the $g(s^*)$ approach works well so long as the analyst choices are appropriate to the goals of the analysis.

Do the g(s) data transformations truly cause nonoptimal fits?*

Brown and coworkers [7] attempted to directly compare PBM fits of the TRAP experimental data with corresponding $g(s^*)$ fits using either the subset of scans used for the "default" $g(s^*)$ fit or a much larger group of scans (13–44). In both cases, their PBM fits gave somewhat different mass and sedimentation coefficient values than the $g(s^*)$ fits, meaning that a PBM analysis that fixes s and M at the best-fit values from the $g(s^*)$ fit will give a higher RMSD than when those parameters are optimized in the PBM fit. From these observations, the authors concluded that the data transformations used in generating the $g(s^*)$ distribution lead to results that are "nonoptimal in the original data space." However, this conclusion is not valid because the comparison is not valid;

these fits are simply not equivalent, and there is no reason to expect that they should give exactly the same best-fit hydrodynamic parameters. There are several reasons why PBM and $g(s^*)$ fits that employ the same group of scans and sedimentation coefficient ranges are not equivalent: (i) the approaches used for removing the TIN are fundamentally different, (ii) the PBM fit is not actually fitting the same portions (same radial ranges) of the scans that are used in computing the $g(s^*)$ distributions, and (iii) the algorithms used in calculating and removing the TIN lead to a different weighting of the raw data between the $g(s^*)$ and PBM fits as well as an artificially low value for the reported RMSD of the PBM fits. Each of these three points also serves to illustrate important (but often poorly understood) differences between these analysis algorithms; therefore, they are explored in detail below.

Differences in systematic noise removal algorithms

One major reason why the PBM and $g(s^*)$ fits cannot be directly compared is that they use fundamentally different approaches for removing the TIN. The scan-differencing approach used in time-derivative analysis removes the TIN arithmetically. This procedure is essentially axiomatic; by definition, any baseline signals that are constant in time (the same in every scan) will be exactly removed by simple arithmetic when raw scans are subtracted in pairs. This TIN removal occurs before the transformation to $g(s^*)$ and is totally independent of any fitting model or its fitting parameters.

The alternate approach used in PBM is to explicitly include in the fitting function an unknown baseline profile (an array of values covering the radial range over which raw data are being fitted) and to optimize this TIN array during the fit. Similarly for interference scans, the systematic vertical displacements between scans (radially independent noise [RIN]) can also be evaluated through an additional set of fitting parameters (one displacement value per scan). As demonstrated by Schuck and Demeler [19], it is possible to separate the linear TIN and/or RIN fitting parameters from the nonlinear hydrodynamic ones and to calculate the TIN and RIN algebraically between each iteration of the hydrodynamic parameters, which greatly speeds the calculations. Nonetheless, the TIN and RIN remain as fitting parameters, and they cannot be determined independently from the other fitting parameters. Furthermore, this procedure will converge to the true TIN (e.g., that obtained from a solvent–solvent blank) only if the fitting model is perfectly correct (if it completely and accurately describes the time-dependent sedimentation of all components that influence the range of data being fitted). The nonequivalence of scan differencing and fitting the TIN was also recently emphasized by Schuck [21].

The fundamental differences between these two approaches automatically means that $g(s^*)$ and PBM fits are nonequivalent and generally should not be expected to give the same best-fit hydrodynamic parameters. Although one cannot directly compare PBM and $g(s^*)$ fits for real experiments where the true TIN is unknown, what happens for simulated data where the TIN is precisely zero? For the default fit of the TRAP simulation, a PBM fit without TIN or zero offset returns a mass of 10.88 subunits, whereas the $g(s^*)$ fit returns a mass of 10.85 subunits. The next section shows that these two fits are not using exactly the same data points from the raw scans and, thus, the best-fit values should not necessarily be identical. Nevertheless, if we substitute 10.85 subunits rather than 10.88 in the PBM fit, the variance increases by only 0.012%, far below the increase of 3.3% needed for statistical significance at only 68.3% confidence. Thus, in the absence of the TIN removal differences, there is no evidence that the $g(s^*)$ result is in any significant way "nonoptimal in the original data space."

Nonequivalence of raw data ranges

A second major reason why the PBM and $g(s^*)$ fits are not directly comparable is that they are not really using the same regions of the raw scans. When calculating $g(s^*)$ distributions via the time-derivative method [4], the scans are first subtracted in pairs and then the radial scale is transformed to a sedimentation coefficient scale using the standard relation

$$S^* = \frac{1}{\omega^2 t^*} \ln \frac{r^*}{r_m} \quad (1)$$

where s^* is the sedimentation coefficient that will produce a boundary at radial position r^* at elapsed run time t^* for angular velocity ω and meniscus position r_m. A subtle but important point is that to achieve removal of TIN, the scans must be subtracted before the transformation to sedimentation coefficient space. However, applying this conversion *after* subtracting the scan pairs requires that a single time t^* must be applied to *both* of the scans in the pair. In contrast, for PBM the t^* of each individual scan is used when the sedimentation coefficient range limits are converted to radial range limits for each scan. In the standard Stafford [8] $g(s^*)$ algorithm, the time assigned to each scan pair is the harmonic mean of the elapsed times for the two individual scans in the pair.[6] Alternatively, in situations where the scans span a large range of boundary movement (much larger than is normally used for time-derivative analysis), it can be advantageous to use the arithmetic mean rather than the harmonic mean to reduce the peak broadening, and that is an option in the DCDT+ program.

This difference in algorithms means that even when the sedimentation coefficient ranges for PBM and $g(s^*)$ fits are the same, the two fits are never derived from exactly the same data points in the raw scans. When the subset of scans used for computing $g(s^*)$ covers only a small range of boundary movement (the normal case), the differences between the mean values for the scan pairs and the actual elapsed times are small. However, when a large range of scans is used (larger than is normally used for time-derivative analysis), this difference can become quite significant and, in fact, this difference is also the major cause of the peak broadening that occurs in such circumstances. A specific example will make these points much clearer, and the analyses of TRAP scans 13–44 in Ref. [7] are used for this purpose. For the first scan pair (scans 13 and 29), the arithmetic and harmonic mean times are 36.1% and 56.5% larger than the actual elapsed time for scan 13 and are 26.5% and 37.1% smaller than the actual time for scan 29, respectively. It appears that the arithmetic mean option was used in Ref. [7], so it is used for the remainder of this example.

Fig. 5A shows that for scan 13, there is a major difference between the true $g(s^*)$ distribution at that time in the run (the solid black curve) and the version that results when the arithmetic mean time is employed in its calculation (dashed blue curve), where every s^* value is only 63.9% of the true value. Consequently, when the fitting region of 4.39–6.28 S is applied (the heavier red region), instead of a region roughly centered on the main peak (the desired limits), the result is a region shifted far to the right side of the main peak, where the data have substantial contributions from the aggregates. Indeed, there is actually zero overlap between the radial portions of scan 13 that contributed to the fitted $g(s^*)$ data in Ref. [7] and the portions that contributed to their PBM analysis with the same fitting limits. Note too that the resolution of the aggregates from the 11-mer at this early time in the run is poor, so that even without the shifting effect, the limits of 4.39–6.28 S would not be effective at excluding the contributions of the 22-mer.

[6] To account for the acceleration period of the rotor, it is really the value of the integral $\int_0^{t^*} \omega^2(t)dt$ (a value that is recorded with each scan) rather than $\omega^2 t^*$ that is used in Eq. (1) and in calculating the mean values applied to the scan pair. For simplicity and brevity, however, this discussion uses "elapsed time" to mean the effective time (i.e., the actual integral divided by the square of the final angular velocity).

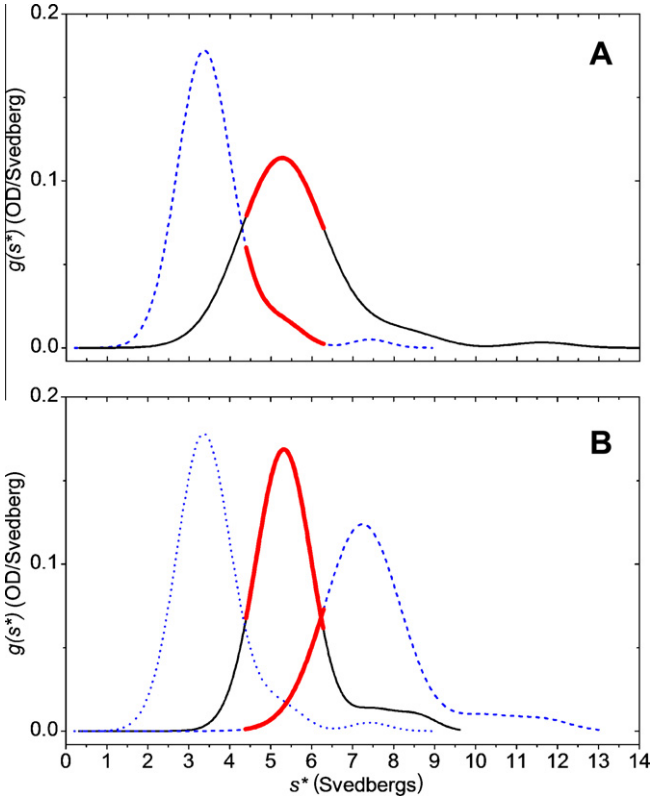

Fig.5. Illustration of the consequences of assigning a single mean run time to both scans in a scan pair. This example uses the actual run times corresponding to the first scan pair from Brown and coworkers' [7] analysis of scans 13 to 44 of the TRAP experiment, but this figure uses simulated data (the same simulation used for Fig. 1B but without added noise). (A) The solid black curve shows the true $g(s^*)$ distribution at the elapsed time of scan 13. The heavier red portion of that curve marks the data within the range from 4.39 to 6.28 S (these are the points derived from the same regions of the raw scan that would be used in PBM analysis with the same fitting limits). The dashed blue curve is the result when the arithmetic mean elapsed time from scans 13 and 29 is used to compute the $g(s^*)$ distribution for scan 13, which rescales the abscissa by a constant factor (and the vertical scale changes as well to keep the area under the curve constant). The heavy solid red portion of the dashed curve shows the portion between the fitting limits of 4.39 and 6.28 S. (B) The solid and dashed curves correspond to those in panel A but apply to the other scan in this pair, scan 29. When the mean time is used rather than the true elapsed time, the true distribution (solid black) is scaled to higher sedimentation coefficients (dashed blue). The dashed blue curve from panel A is shown as a dotted line to help illustrate why the net contributions of this scan pair to the final $g(s^*)$ distribution will produce severe broadening of the peaks. (For interpretation of the references to color in this figure legend and the text, the reader is referred to the Web version of this article.)

As shown in Fig. 5B, the true distribution for scan 29, the other scan in the pair, gets distorted in the opposite way. Thus, when the fitting limits are applied, the result is data derived entirely from the left side of the main peak. For this scan, there is a small overlap (~16%) between the regions of the scan that would contribute to a PBM fit and those that will contribute to the $g(s^*)$ fit. Fig. 5B also illustrates why the use of large subsets of scans (large ranges of boundary movement) produces severe broadening of the peaks in the $g(s^*)$ distribution. When the contributions of scan 13 (the dotted blue curve in Fig. 5B) get averaged with those from scan 29 (dashed blue curve), the result would actually give a split main peak. However, when the contributions from the other scan pairs get added, the net result is a severely broadened main peak rather than a split one.

PBM fits can produce an unintended effect that some raw data points have no influence on the results

A third important reason why PBM and $g(s^*)$ fits that use the same scans and sedimentation coefficient ranges are nonequivalent is that the fitting of the TIN during PBM has the unintended consequence of weighting the raw data unevenly. Indeed, it turns out that some of the data points from scans early in the run have zero influence on the fit (their weight is zero), whereas others have significantly less than full weight. This effect arises because the sedimentation coefficient limits also severely limit the extent to which the data from successive scans overlap in radius. Therefore, at some radial positions, there may be very few scans (as few as 1 scan) that contribute to determining the TIN for that radius. Such data points turn out to have little (or even no) influence on the fit.

This can be easily demonstrated by an example. Fig. 6A shows the scans from the TRAP simulation in the region near the meniscus, with those data points that are actually included in a PBM fit covering the usual range of 4.39–6.28 S marked as red diamonds. Note that only a single data point from the first scan gets fitted and that there is no radial overlap of the fitted regions until a partial overlap occurs for the fourth (and later) scans. The red solid lines in Fig. 6A and B show the fitted curves and residuals from a PBM fit of all the scans. The fitted curves go exactly through those data points where there is no overlap with other scans, and those residuals are zero (within round-off error). The points shown as green open circles and the dashed green lines show the results for a refit after certain data points were manually shifted upward by 0.15 OD (an arbitrary amount). The fit of the altered scans returns the same fitting parameters and RMSD, and once again the fit goes exactly through those altered data points. The same result would be obtained no matter what OD is assigned to those particular data points; they have zero influence on the fit results. Most of the other data points from the early scans also have less than normal influence on the fit, and their residuals are also suppressed below the values expected from the random noise added to this simulation, but those effects are not obvious by inspection of Fig. 6.

Why do these things happen? They are actually implicit in the formula for calculating the TIN. If the RIN is zero (as is normally assumed for absorbance scans), Eq. (7) from Ref. [7] for the TIN at the radial position given by index j can be rewritten as

$$b_j = \frac{1}{M_j}\sum_{i=1}^{M_j}(y_{i,j} - F_{i,j}), \tag{2}$$

where M_j is the number of data points being fitted at that radial position, $y_{i,j}$ is the ith experimental data point being fitted at radial index j, and $F_{i,j}$ is the total Lamm solution fitting function (the sum of the theoretical boundaries for all of the species being fitted) for that experimental point.[7] Eq. (2) shows that the TIN at each radius is simply the mean value of the difference between the experimental point and the theoretical boundary computed for all of the fitted points at that radius. In other words, the TIN is chosen to make the mean residual at each radius be zero.

This means that at any radial position where only a single data point is being fitted, the residual should always be exactly zero. That is indeed what is observed except that in practice there appears to be some round-off error, so the residuals are not always precisely zero. Moreover Eq. (2) also implies that at any radial position where only a small number of points are being fitted, the effect of fitting the TIN is to significantly reduce the influence of such points on the overall variance of the fit (such points have a less than normal weight). To see this, using the notation of Eq. (2), the formula for χ^2 becomes

$$\chi^2 = \sum_j \sum_{i=1}^{M_j}[y_{i,j} - (F_{i,j} + b_j)]^2. \tag{3}$$

[7] In the notation of Brown and coworkers [7], $F_{i,j} = \sum_k c_k L_{i,j}^{(k)}$.

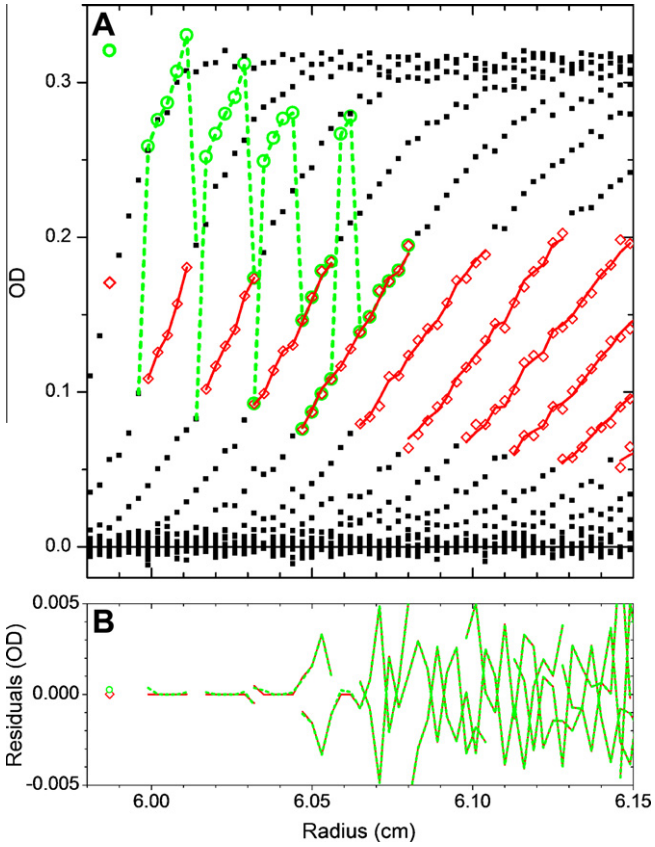

Fig.6. Effects of fitting the TIN for nonoverlapping data points. (A) The small black filled squares show scans taken from the TRAP data simulation used in generating Figs. 1B and 4B. The red open diamonds show the data points that are included for a PBM fit of all 67 scans using fitting limits of 4.39 to 6.28 S, and the red solid lines show the actual fitted curves from that fit (for the first scan, only a single data point is included in the fit, so that point is shown as a diamond). The green open circles represent an alternate data set where the points that do not overlap with other scans (those radial positions for which only a single data point is included in the fit) were arbitrarily shifted upward by 0.15 OD (only the shifted points are shown; the other data points in this alternate data set are identical to the squares or diamonds). This alternate data set was also fitted by PBM analysis, and those fitted curves are shown in dashed green. (B) The residuals from the fits of the normal and alternate (certain points shifted) data sets are shown as solid red and dashed green lines, respectively. (For interpretation of the references to color in this figure legend and the text, the reader is referred to the Web version of this article.)

Differentiating with respect to any single data point y_{ij}, substituting $\partial b_j/\partial y_{i,j} = 1/M_j$, and rearranging gives

$$\frac{\partial \chi^2}{\partial y_{i,j}} = 2(y_{i,j} - F_{i,j} - b_j)\left(1 - \frac{1}{M_j}\right). \quad (4)$$

This shows that for any point where $M_j = 1$, the derivative vanishes identically (that point has no influence on the least squares fit), but it also implies that when M_j is a small number, fitting the TIN will cause those points to have significantly less influence on the fit. Consider the increment to χ^2 contributed by all the points at radius index j, $\Delta\chi_j^2$:

$$\Delta\chi_j^2 = \sum_{i=1}^{M_j}(y_{i,j} - F_{i,j} - b_j)^2. \quad (5)$$

After substituting Eq. (2) and rearranging, this can be written as

$$\Delta\chi_j^2 = \sum_{i=1}^{M_j}(y_{i,j} - F_{i,j})^2 - \frac{1}{M_j}\left[\sum_{i=1}^{M_j}(y_{i,j} - F_{i,j})\right]^2. \quad (6)$$

The first sum on the right side in Eq. (6) is simply the χ^2 increment that would occur if the TIN were not subtracted. Because the squared sum in the second term must be positive, the effect of fitting the TIN is always to reduce the net increase in χ^2. The inverse dependence on M_j for the second term means that this reduction is relatively large when M_j is small but goes asymptotically to zero as M_j becomes large (as the number of overlapping scans becomes large). For PBM fits, it will always be true that the overlap of the boundary between successive scans is much less early in the run, meaning that fitting the TIN will always give data points from the early scans a lower weight relative to the late scans.

The number of data points with zero or low weighting becomes especially large when using an 8-hole rotor for absorbance scans. For a new simulation of the TRAP experiment assuming that 7 cells in an 8-hole rotor were scanned (increasing the scan interval by 7/3), when the first half of the run was fitted by PBM, 67 of the 347 total data points have residuals that are always zero. The RMSD of this fit is returned as 0.002612 OD, far below the value of 0.003580 OD that should be observed (the true noise added to the simulation). Clearly, this side effect of fitting the TIN with PBM fits can seriously distort the fit statistics (the difference between the observed and expected RMSD values is statistically significant with $P < 10^{-7}$). More important in the current context, the different effective weighting for different data points is yet another reason why PBM and $g(s^*)$ fits are inherently different and should not necessarily give the same best-fit hydrodynamic parameters.

Although Brown and coworkers [7] did state that for PBM fits it is important to have overlapping scans, and that at least two scans must contain data at each radius for fitting the TIN, they did not apply that rule in their analyses of the TRAP data. Furthermore, even if the early scans are excluded to ensure overlap, it is still true that fitting the TIN greatly reduces the effective weight of points for which the number of scans is low, and that important consequence has not been described previously.

With respect to weighting of data points, it should be clarified that the $g(s^*)$ fits are in fact normally weighted fits (and should be). The data transformations cause the $g(s^*)$ points at low sedimentation coefficients to have a higher uncertainty than those at higher sedimentation coefficients. That systematic effect is properly accounted for by the default weighting, which assumes that the intrinsic noise in the raw scans is independent of radial position. The need for weighted fits can be avoided, if desired, by fitting directly to the dc/dt data rather than $g(s^*)$ [6].

To conclude this section, it has been shown that there are three independent reasons why "equivalent" $g(s^*)$ and PBM fits are actually not equivalent and, therefore, the best-fit parameters from one approach should not be optimal in the other. Each approach is "nonoptimal" in the other's data space, and each is correct for its own.

PBM fits can give physically unrealistic estimates for the TIN that distort the results

The PBM fits for this study also reveal that the computed TIN often becomes physically unrealistic (i.e., it deviates significantly from the scans that were recorded after all components have sedimented past that position). This is especially true at low radii, where the TIN values are being derived from early scans. Fig. 7A shows three different estimates for the TIN from the TRAP experiment. The green solid curve is an average of the last 20 scans (48–67) over the region out to 6.75 cm where the cell had already been depleted of all protein. That is, the green curve is essentially a model-independent experimental TIN covering the region below 6.75 cm. The red dashed curve is the TIN computed for the PBM fit of all 67 scans, which clearly deviates significantly from the green curve. The deviation of this TIN from the actual scans at times after the cell is empty can also be seen in Fig. 4a of Ref. [7]. The blue dotted curve is the TIN computed from the hybrid-

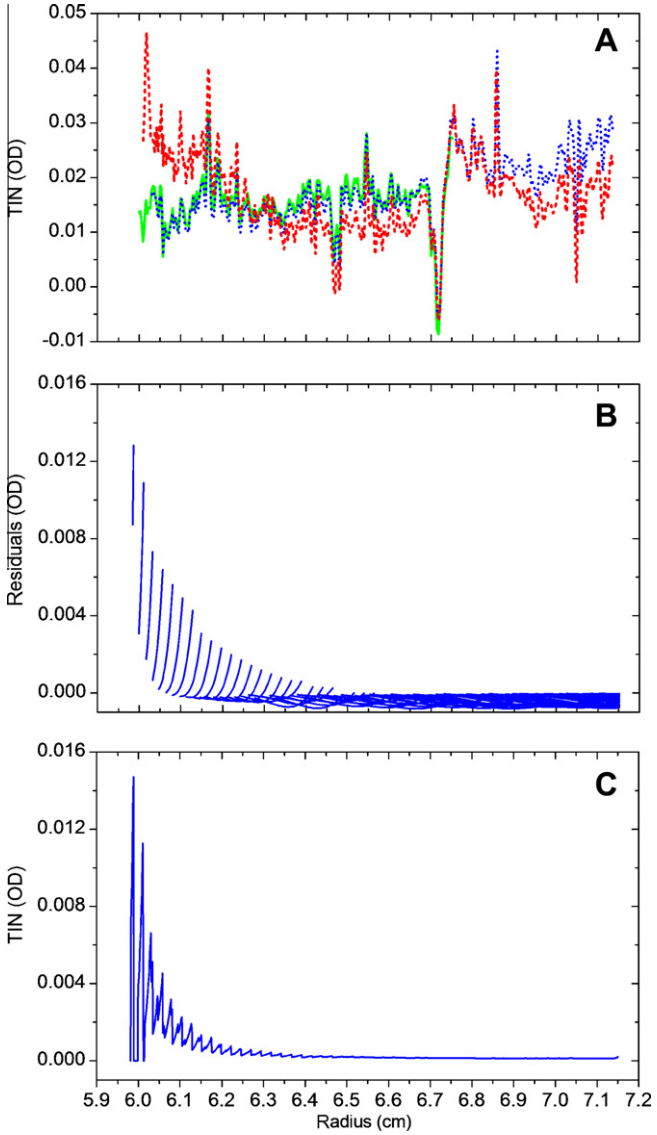

Fig.7. (A) Estimates of the TIN for the TRAP experiment. The green solid curve is the average of the last 20 scans (out to 6.75 cm), the red dashed curve is the TIN derived from the PBM fit of all 67 scans, and the blue dotted curve is the TIN derived from the hybrid-discrete model fit of all 67 scans. (B) Residuals resulting when a noise-free simulation of the TRAP experiment is fitted by PBM (range of 4.39–6.28 S with the TIN held at zero) as a single species with the known (as simulated) values for the main component. (C) The TIN computed from a single-species PBM fit (range of 4.39–6.28 S with the TIN floated) of the same noise-free simulation used for panel B. (For interpretation of the references to color in this figure legend and the text, the reader is referred to the Web version of this article.)

discrete model fit of all scans in Ref. [9], which is in good agreement with the solid green curve at the radii covered by both. These seemingly subtle differences in the TIN can have a substantial impact on the analysis results. For example, for the PBM analysis of scans 13–44 discussed in Ref. [7], if the TIN from the hybrid-discrete model fit is used rather than the best-fit TIN, this changes the best-fit mass from 10.50 to 11.89 monomer units.

Why does a PBM fit give a TIN that differs from an experimental baseline or the TIN computed from a model that considers all species and uses all scans? The key point is that the purpose of the PBM fit is to try to exclude the influence of species that are present in the sample but are not of interest. However, that means that the PBM model is fundamentally an incorrect description of the sample, and if it fails to sufficiently exclude the influence of the other species, there will inevitably be systematic deviations between the data and the fit. Fig. 7B shows the residuals that result from modeling a noise-free version of the TRAP simulation as a single species by PBM using (i) the sedimentation coefficient range of 4.39–6.28 S from the default $g(s^*)$ fit, (ii) the actual main peak (11-mer) parameters from the simulation, and (iii) a TIN fixed at zero (the correct value). The nonzero residuals clearly show that the PBM limits are not able to completely exclude the effects of the aggregates, especially for the early scans (where the aggregates are not yet resolved from the main boundary). Thus, a correct fit of these data should *not* return exactly the true mass of the 11-mer; some portion of the true heterogeneity of the sample remains in the data being fitted, and so that heterogeneity should result in an estimated mass that is *lower* than that of 11-mer. If these same noise-free data are fitted by PBM allowing fitting of the TIN, however, the returned mass estimate is 11.04 subunits, slightly *above* the correct value, and the TIN that is returned (shown as Fig. 7C) is a physically unreasonable spiked or sawtooth pattern (and definitely not the known value, zero everywhere). This patterned TIN does succeed at mostly removing the systematic residuals that arise from the extra species; it reduces the maximum residual approximately 4-fold and decreases the RMSD more than 2-fold. That is, the extra degrees of freedom provided by the TIN substantially reduce the sensitivity of the fit to the fact that the model does not account for all of the species that are actually present.

Does including the early scans or fitting the meniscus position significantly improve the results of PBM fits?

Two other points emphasized by Brown and coworkers [7] were that the ability to include all of the scans in a PBM analysis and also to include the meniscus position as a fitting parameter are important advantages over fitting $g(s^*)$ distributions. However, the model PBM analyses of their BSA experiment (Fig. 5 in Ref. [7]) never included all of the scans and did not show any substantial improvement in accuracy for a fit using scans 10–69 versus one using only scans 58–69. Furthermore, they did not investigate whether inclusion of all scans significantly improves the precision of the fitted parameters for either the TRAP or BSA experiments. In fact, as shown by the open black diamonds in Fig. 1B, PBM fits of the simulated TRAP data show no difference in the shape of the error surface between fits using only scans 29–67 (after the main boundary had reached the midpoint of the cell) versus the fit using all of the scans (the solid green curve). That is, the inclusion of the first half of the run does not produce a sharper minimum in the error surface. Furthermore, the error surface for this scan fit (29–67) is virtually unchanged whether the meniscus position is included as a fitting parameter or held fixed at the known position (filled black squares). This shows that fitting the meniscus position improves neither the accuracy nor the precision of the fitted mass. Conversely, it shows that even when no early scans are included, the additional freedom associated with allowing the meniscus position to float is also not significantly detrimental to the precision of the mass determination.

Similarly, the PBM fits of the BSA experiment simulation also provide no evidence that inclusion of all the scans improves the results. The dashed blue curve in Fig. 2A shows the fit quality profile for a fit using only scans 34–69 (starting from the time the monomer has reached the midpoint of the cell). Because the number of fitted data points is lower, the critical χ^2 levels are, of course, slightly higher for this fit than for the fit using scans 10–69 (solid green curve). However, because the minimum is actually somewhat sharper for the fit using fewer scans, the width of the 95% confidence intervals is nearly identical (total range of 20.2 kDa for scans 10–69 and 20.4 kDa for scans 34–69).

A modified time-derivative algorithm can limit the g(s) peak broadening when a large range of boundary movement is used and can improve the isolation of specific species of interest*

There is no dispute that the peak broadening of $g(s^*)$ distributions derived from a large range of boundary movement is a limiting factor for fitting $g(s^*)$ distributions of samples containing multiple species. This drawback can also make it difficult to analyze samples containing a relatively large range of sedimentation coefficients. It appears, however, that there is some misunderstanding about whether and when the "improved algorithm" for fitting $g(s^*)$ distributions [9] should reduce or eliminate this drawback [7]. For samples containing only one species, this algorithm does make the peak broadening irrelevant, but for multispecies samples, the peak broadening will still have a negative impact on the ability to resolve multiple components, as was explicitly stated and illustrated in Ref. [9].

In practice, however, limiting the range of boundary movement to avoid substantial peak broadening is often not a significant drawback. The results from the $g(s^*)$ fitting of the TRAP simulation (Fig. 5B) demonstrate that the peak broadening can easily be kept low enough such that the correct stoichiometry is obtained and that nonetheless the signal/noise ratio is high enough to define the stoichiometry within ±0.5 subunit for a fairly broad range of scan subset choices. The 15 antibody measurements (Fig. 3) also show that a mass estimate with a relative standard deviation below 1% can be obtained using only 16 scans (giving no significant peak broadening for species below ~350 kDa).

Is there a way to reduce the peak broadening in those situations where it is significantly limiting? Fortunately, a range of boundary movement large enough to cause substantial broadening also increases the signal/noise ratio of the scan difference curves, and that in turn permits a new alternate approach to calculating dc/dt where the signal/noise ratio is traded off for increased resolution (lower peak broadening).

In the standard dc/dt algorithm where, for example, a total of 16 scans are being analyzed, scan 9 is subtracted from scan 1, scan 10 is subtracted from scan 2, . . ., and scan 16 is subtracted from scan 8. This differencing pattern results in scan differences with the highest signal/noise ratio, but it is not an intrinsic requirement of this approach. If instead these 16 scans were first divided into 2 continuous sections, and the usual pattern then applied to each of those 2 sections, one could pair the scans as follows: (5, 1) (6, 2) (7, 3) (8, 4) (13, 9) (14, 10) (15, 11) (16, 12). This alternate pairing will reduce the maximum time difference between the scans in a pair by 2-fold and can reduce the peak broadening effects by as much as 4-fold [6], but at a penalty of a 2-fold reduction in the signal/noise ratio of the resultant $g(s^*)$ distribution. Importantly, this alternate pairing retains the property that each scan is used only once, avoiding the statistical issues that arise for some other differencing patterns that were proposed recently [21]. This sectioning process could continue down to a minimum of 4 scans per section. This approach is not restricted to even numbers of sections and can be applied to arbitrary total numbers of scans, but in the general case one section will have a larger number of scan pairs than the rest of the sections. In such cases, it is advantageous to group scans such that the section with the most scans is the last one (highest scan numbers) because peak broadening will be least important for that group.

Fig. 8 illustrates applying this new approach to a broad range of scans from the TRAP experiment (13–44), a group that was also analyzed in Ref. [7]. The standard $g(s^*)$ one-segment distribution shows extensive broadening of the main peak, resulting in very poor resolution of the main peak from a shoulder caused by the aggregates sedimenting at approximately 7.5 and 8.6 S. By visual inspection, it seems obvious that the fitting limits of 4.39–6.28 S (the vertical dashed lines in Fig. 8) will not succeed in isolating the properties of the main peak from the shoulder of aggregates, so it is not surprising that the single species fit returns a mass of 8.6 monomer units rather than 11 [7]. Note too that for this case the DCDT+ program displays a "peak broadening limit" (the approximate mass above which the peaks will be significantly broadened [9]) of only 8.8 kDa (an order of magnitude below the 11-mer mass). However, with this new algorithm, the peak broadening can be substantially reduced for the same scan selection. The main peak sharpens significantly in going to 2 and then 3 sections, but there is little further improvement in going from 3 to 4 sections or going from 4 to 6 sections. Going to 8 sections only further degrades the signal/noise ratio. At 4 sections, the peak broadening limit (the lowest value for any of the 4 sections) has been increased to 77 kDa (roughly 9-mer), consistent with the limited sharpening of the main peak from going beyond 4 sections. Although using multiple sections clearly does help, the resolution of the aggregates from the main peak is still never good because ultimately it is limited by the fact that the aggregates were not yet resolved from the main peak at the time of the earliest scans included in this group. Consequently, a fit of the TRAP simulation using 4 sections with scans 13–44 gives a mass of 10.90 subunits, ~1% below the true value. Importantly, this multisection approach does give the correct stoichiometry, and with sufficient precision to exclude other stoichiometries (Monte Carlo 95% confidence of 10.63–11.17 subunits), from a very broad range of scans that otherwise gives quite poor results.

Using scan differencing with PBM

This multisection algorithm for scan differencing also makes possible a new approach to removal of TIN for PBM fitting. Although scan differencing has been used for TIN removal in whole boundary fitting for many years in the programs SVEDBERG [15] and SEDANAL [22], applying sedimentation coefficient limits to the difference data is usually not possible when the standard single-section scan pairing is used. The only radial points that can be differenced in each scan pair are those for which the partial boundaries overlap. Good overlap requires that the boundary has not moved very far between the scans being differenced, especially when the sedimentation coefficient limits are narrow. However, for whole boundary analysis, the full range of boundary movement is typically used in the analysis, and with the standard differencing

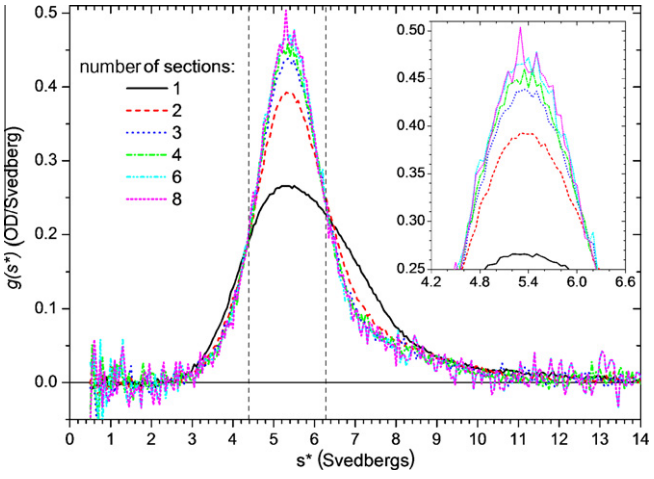

Fig. 8. $g(s^*)$ distributions from scans 13 to 44 of the TRAP experiment with this group of scans divided into different numbers of sections. The dashed vertical lines indicate the fitting limits of 4.39 to 6.28 S that were applied in Brown and coworkers' [7] analysis of this group of scans. The inset shows an expanded view of the top of the main peak.

pattern this means that the boundary has moved nearly half the length of the cell between the two scans being subtracted; hence, there is no overlap of corresponding regions in both radial and sedimentation coefficient space. The multisection differencing pattern greatly increases the overlap, and that algorithm has now been implemented for PBM analysis in the program SVEDBERG. Using multiple sections, unfortunately, creates a penalty of lower signal/noise ratio for the difference data, just as in $g(s^*)$ analysis. Furthermore, the requirement for radial overlap means that the effective sedimentation coefficient limits are actually somewhat more restricted than the desired values for one scan or the other in each pair. More sections increase the overlap, so more difference points remain in the fit, but those points will have a lower signal/noise ratio.

To illustrate this alternative approach to PBM fitting, it has been applied to the BSA simulation discussed previously. A fit exactly analogous to the PBM fit with TIN using SEDPHAT (Fig. 2) was done using scan differencing with 10 sections (6 scans each). That fit gives a BSA monomer mass of 67.71 kDa (2.0% above the correct value), and Monte Carlo analysis using the known noise level of the simulation gives 95% confidence limits of 65.18–69.20 kDa (−1.8 to +4.3%). Thus, this scan-differencing approach to PBM fitting gives similar accuracy to PBM done with SEDPHAT, but the alternate approach to handling TIN removal has reduced the mass uncertainty 5-fold (and has given a precision equivalent to that of the $g(s^*)$ fit using 14 scans). Although a similar fit using 6 sections rather than 10 sections gives scan differences of higher magnitude, the lowered overlap between scans yields fewer net data points in the fit, and the precision of the fitted mass is essentially the same.

General discussion

Advantages and drawbacks of the PBM approach

Some significant advantages proposed for the PBM approach, according to Brown and coworkers [7], are that it "allows the inclusion, without drawbacks, of all available scans" and also "allows one to use very large or entire data sets without drawbacks. This is unbiased and statistically optimal." Those claims, however, are not consistent with the findings here or, indeed, with the author's stated requirements of the method.

First, it is not always possible to use all available scans when the meniscus position is fitted. As mentioned earlier, when scans very early in the run are included, attempting to fit the meniscus position often results in error messages. Presumably, this is why the PBM fits of the BSA experiment in Ref. [7] never included scans earlier than scan 10. Second, when the TIN is being fitted, the inclusion of scans very early in the run inevitably leads to the problem of data points that have zero weight (Fig. 6) as well as substantial numbers of data points that are significantly underweighted (as shown by Eq. 6). These effects consistently led to PBM fits of simulated data giving an RMSD significantly below the true noise level in the simulations.

It is true that PBM fits can include a larger fraction of the scans than $g(s^*)$ fits even when the latter uses the new multisection approach. And clearly, the use of all or most of the scans seems to be statistically preferable *in theory*. However, it was never actually demonstrated that *in practice* inclusion of all the scans does provide a significant advantage. The tests done here (Figs. 1B and 2A) indicate that inclusion of the scans prior to the time when the main boundary reaches the middle of the cell in the PBM analyses does not significantly improve either the accuracy or the precision of the fitted parameters. One reason why early scans have relatively low influence on PBM fits is simply because they contribute few data points (see Figs. 2 and 6), and the statistical weighting issues uncovered here reduce their impact even further.

The PBM approach also can give very broad minima in the error surface (such as those shown in Figs. 1 and 2A). Those broad error surfaces led Brown and coworkers [7] to conclude that "it is apparent the data [the TRAP raw data] simply do not have the information to determine the oligomer size." However, that conclusion is not consistent with (i) any of the three different approaches to estimating the parameter precision for the "default" $g(s^*)$ fit of 12 scans or (ii) the results from the new 4-section $g(s^*)$ fit covering scans 13–44, (iii) the results from the $g(s^*)$ fits of the TRAP simulation (Figs. 1B and 4B), or (iv) the earlier hybrid-discrete model analysis using all of the scans [9]. That is, the statistical properties of the PBM approach led to an incorrect conclusion that the data were inadequate to answer the question being posed.

These broad error surfaces are also a major reason why PBM fits often show poor convergence. Brown and coworkers [7] themselves described the error surface for their scan 13–44 PBM fit of the TRAP data as "ill-defined" and noted the poor convergence. When this same fit was repeated here, but instead using the simulated annealing method to find the minimum, a reproducible convergence was obtained; interestingly, however, that fit produced a lower RMSD than was reported (0.00470 vs. 0.00474 OD) and the best-fit stoichiometry shifted from 9.7 to 10.7 subunits. All of the observations discussed in this section seem to be inconsistent with the claims for a "statistically optimal" method.

Brown and coworkers [7] further stated that "the key advantage of the PBM approach is that it naturally allows ... all unknowns to be included into the analysis." Clearly, the ability of PBM to fit the meniscus position can be useful and will often result in fits with a lower RMSD, and the inability to fit the meniscus position is indeed a drawback of $g(s^*)$ analysis. But it has not been demonstrated that in practice fitting the meniscus produces results that are more accurate or more precise either for PBM fits [7] or for whole boundary analysis in general. Fig. 1B shows that fitting the meniscus has no significant influence on the determination of the mass even when no early scans are included in the analysis and, therefore, the meniscus position is poorly constrained. Fitting the meniscus position does indeed provide a direct way to evaluate the influence of the meniscus position on the other parameters. However, it is also straightforward to evaluate whether the results from $g(s^*)$ fits are highly sensitive to the chosen meniscus position by manually varying the value over a physically realistic range and refitting, and such testing gave changes in the apparent mass of only 1% for the TRAP simulation.

Moreover, a fundamental problem arises for any method that simultaneously fits the meniscus position while also trying to restrict the range of sedimentation coefficients being fitted. Clearly, the meniscus position strongly affects the apparent sedimentation coefficient associated with each radial position (Eq. 1). Thus, in principle, during PBM analysis, as the meniscus position is varied during fitting iterations, the actual raw data being fitted should also change to keep the sedimentation coefficient range constant. Such readjustment of the fitted data after each iteration is, however, not compatible with standard least squares fitting algorithms and is not actually implemented for PBM analysis. In practice, the lack of such readjustment of the raw data ranges probably has only a small effect on the final results but, at a minimum, makes it difficult to reproduce the same raw data range (the range will depend on the initial value assumed for the meniscus position, not the final best-fit value).

Although Brown and coworkers [7] stated that PBM allows automatic evaluation of the effect of all important parameters and analyst choices on the fitting results, in fact it cannot evaluate how the choice of the sedimentation coefficient range to be fitted changes the outcome. That sedimentation coefficient range is manually preselected for both the PBM and $g(s^*)$ approaches, and a poor choice (e.g., one that fails to exclude the contributions of

the unwanted species) will adversely affect the results for either approach. For $g(s^*)$ fitting, the width of the peak provides a natural guide for making this range selection and directly shows the quality of the separation, and the antibody data in Fig. 3 prove that the approach of using the 50% peak height to pick the fitting range does give consistent results. On the other hand, no such guidance for range selection is provided by the PBM approach.

Fitted TIN versus scan differencing

With respect to removal of baselines, Brown and coworkers [7] argued that (i) fitting the TIN is superior to scan differencing because the "pairwise subtraction method is more permissive to small drifts (since the first pair does not need to have the same TI noise as the last pair)" and (ii) fitting the TIN and scan differencing "have similar degrees of freedom (or 'model dependence')." This first claim is simply illogical; by definition TIN must be the same in every scan (and, therefore, in every scan pair), and by definition a drift over time is not time independent.

The second claim is readily disproved. Fitting the TIN requires, at a minimum, hundreds of fitting parameters, and can require up to ~1600 parameters for interference scans. Removal of the TIN via scan differencing requires none, and the result of the differencing is completely fixed once the scans are recorded and the scan subset is selected. Figs. 2B and 7A directly demonstrate this fundamental difference between fitting the TIN and removing it via scan differencing; the fitted TIN changes as the fitting parameters change, leading to changes in the net signal (the data to be modeled by the Lamm equation solutions). In contrast, the net data created by scan differencing are constant and independent of any fitting model; in particular, they remain constant during evaluation of the error surface for the fitting parameters. That is the basis, and the specific meaning, of statements here and in Ref. [9] that scan differencing is "model independent," whereas fitting the TIN is "model dependent." The recent exploration of this issue by Schuck [21] used a different meaning for "model dependence" and gave no results that contradict the meaning used here.

Both this study and Ref. [21] agree that the two approaches to baseline removal will produce different error surfaces for the hydrodynamic parameters. However, the conclusion that scan differencing will always result in larger parameter uncertainty than directly fitting the TIN [21], which was based on a model of fitting data to straight lines rather than fitting actual velocity data or simulations, seems to be contradicted by several results presented here, including those from the new multisection scan-differencing approach for PBM fits as well as from $g(s^*)$ fits. There is no dispute that scan differencing always imposes a statistical penalty because the differenced data have a somewhat higher noise level. However, using the differenced data avoids the statistical penalties associated with needing to explicitly determine the baseline profile and the hundreds to thousands of extra fitting parameters needed to do so. In the specific case of PBM fits, the situation for fitting the TIN is substantially different from that in standard whole boundary analysis because (i) the ratio of total fitting parameters to total data points in the fit is much higher for PBM and (ii) the number of scans contributing to the TIN computation at each radius is substantially less (by an order of magnitude in many cases). For PBM fits, determining the TIN appears to often be a rather ill-conditioned problem, and in practice the statistical penalty associated with fitting the TIN appears to be substantially higher than that associated with scan differencing.

Inherent limitations of fitting a small portion of a boundary

A fairly high cross-correlation between the fitted concentration and the fitted mass appears to be an inherent drawback to fitting a fairly restricted portion of a boundary either directly through the PBM approach or via the transformed $g(s^*)$ distribution. For example, for the "default" $g(s^*)$ fit of the TRAP simulation, both the fit covariance matrix and the Monte Carlo simulations imply a cross-correlation coefficient of −0.88. Therefore, any fitting approach that makes the zero reference for the concentration less certain (e.g., a baseline offset parameter or fitted TIN and/or RIN) will tend to lower the precision with which the mass can be determined. Brown and coworkers [7] also noted that an inability to define the loading concentration is a "potential pitfall" of PBM fits that use a sedimentation coefficient range that is too narrow. However, they did not explore the impact of using a fitted TIN on the ability to define the concentration or the coupling of that concentration uncertainty to the precision of the fitted mass. The results presented here (especially in Fig. 2B) suggest that these factors play a major role.

The need to have a well-determined concentration to obtain a well-defined mass from these partial boundary fits may present serious difficulties for experiments using interference scans where the zero concentration reference varies from one scan to the next. Some limited tests using the TRAP or BSA simulations indicate that fitting RIN in addition to TIN for those PBM analyses would significantly decrease the precision of the mass determination. For $g(s^*)$ analysis, the RIN is usually removed by aligning the fringes at a radius where nothing is sedimenting, and this also may lead to some uncertainty in the true zero reference. Therefore, some further assessment of the reliability of both PBM and $g(s^*)$ analyses with interference data (actual experiments rather than simulations) is probably needed.

Application to reversible associations

Although sedimentation velocity has been widely used to determine the stoichiometry of tightly associated oligomers and multicomponent complexes, there has been little explicit discussion of what "tightly associated" means or how to experimentally test whether the concentration is high enough that the sample can be approximated as a mixture of independent components (i.e., the reversible dissociation can safely be ignored). Because this situation represents a major application for the $g(s^*)$ and PBM approaches discussed here, it is highly pertinent to briefly discuss this issue.

Simulations of rapidly reversible monomer–octamer and monomer–dimer systems were conducted and analyzed by $g(s^*)$ fitting (see Supplementary material for detailed results and figures). In summary, those simulations indicate that the correct stoichiometry can be obtained (error <0.5 subunit) whenever the loading concentration is at least 50-fold higher than the concentration where the monomer and oligomer are equimolar. Under such conditions the sedimentation coefficient of the oligomer is determined with accuracy of better than 1.5% for octamer or better than 4% for dimer.

Usually, however, the experimenter will not know the dissociation constant and must run a dilution series to show that the sample is behaving essentially as a mixture (approximately independent of concentration). The simulations indicate that the results at the higher concentration will be reliable (correct stoichiometry) when a 3-fold dilution produces a decrease in the apparent mass of the oligomer of less than 10% and a reduction in its sedimentation coefficient of less than 0.3%. Although these results apply specifically to $g(s^*)$ analysis, the situation for other data analysis approaches should be similar.

Conclusions

Overall, it is clear that the PBM and $g(s^*)$ approaches both have drawbacks as well as strengths. Hopefully, the additional information from this study will help analysts with method selection and

interpretation of the results and also will clarify a number of issues that apply much more broadly to sedimentation velocity data analysis methods. The new algorithms introduced here also augment and expand the capabilities of both the $g(s^*)$ and PBM methods.

Acknowledgment

This work was supported by Alliance Protein Laboratories and John Philo, software consultant.

Appendix A. Supplementary data

Supplementary data associated with this article can be found, in the online version, at doi:10.1016/j.ab.2011.01.035.

References

[1] P. Schuck, Size-distribution analysis of macromolecules by sedimentation velocity ultracentrifugation and Lamm equation modeling, Biophys. J. 78 (2000) 1606–1619.
[2] P.H. Brown, P. Schuck, Macromolecular size-and-shape distributions by sedimentation velocity analytical ultracentrifugation, Biophys. J. 90 (2006) 4651–4661.
[3] E. Brookes, W. Cao, B. Demeler, A two-dimensional spectrum analysis for sedimentation velocity experiments of mixtures with heterogeneity in molecular weight and shape, Eur. Biophys. J. 39 (2010) 405–414.
[4] W.F. Stafford, Boundary analysis in sedimentation transport experiments: a procedure for obtaining sedimentation coefficient distributions using the time derivative of the concentration profile, Anal. Biochem. 203 (1992) 295–301.
[5] W.F. Stafford, Rapid molecular-weight determination by sedimentation-velocity analysis, Biophys. J. 70 (1996) MP452.
[6] J.S. Philo, A method for directly fitting the time derivative of sedimentation velocity data and an alternative algorithm for calculating sedimentation coefficient distribution functions, Anal. Biochem. 279 (2000) 151–163.
[7] P.H. Brown, A. Balbo, P. Schuck, On the analysis of sedimentation velocity in the study of protein complexes, Eur. Biophys. J. 38 (2009) 1079–1099.
[8] W.F. Stafford, Boundary analysis in sedimentation velocity experiments, Methods Enzymol. 240 (1994) 478–501.
[9] J.S. Philo, Improved methods for fitting sedimentation coefficient distributions derived by time-derivative techniques, Anal. Biochem. 354 (2006) 238–246.
[10] C.A. Brautigam, Y. Chelliah, J. Deisenhofer, Tetramerization and ATP binding by a protein comprising the A, B, and C domains of rat synapsin I, J. Biol. Chem. 279 (2004) 11948–11956.
[11] P.W. White, A. Pelletier, K. Brault, S. Titolo, E. Welchner, L. Thauvette, M. Fazekas, M.G. Cordingley, J. Archambault, Characterization of recombinant HPV6 and 11 E1 helicases: effect of ATP on the interaction of E1 with E2 and mapping of a minimal helicase domain, J. Biol. Chem. 276 (2001) 22426–22438.
[12] Z. Sun, K.B. Reid, S.J. Perkins, The dimeric and trimeric solution structures of the multidomain complement protein properdin by X-ray scattering, analytical ultracentrifugation, and constrained modelling, J. Mol. Biol. 343 (2004) 1327–1343.
[13] N. Mucke, T. Wedig, A. Burer, L.N. Marekov, P.M. Steinert, J. Langowski, U. Aebi, H. Herrmann, Molecular and biophysical characterization of assembly-starter units of human vimentin, J. Mol. Biol. 340 (2004) 97–114.
[14] J.S. Philo, T.H. Yang, M. LaBarre, Re-examining the oligomerization state of macrophage migration inhibitory factor (MIF) in solution, Biophys. Chem. 108 (2004) 77–87.
[15] J.S. Philo, An improved function for fitting sedimentation velocity data for low-molecular-weight solutes, Biophys. J. 72 (1997) 435–444.
[16] A.A. Antson, A.M. Brzozowski, E.J. Dodson, Z. Dauter, K.S. Wilson, T. Kurecki, J. Otridge, P. Gollnick, 11-Fold symmetry of the *trp* RNA-binding attenuation protein (TRAP) from *Bacillus subtilis* determined by X-ray analysis, J. Mol. Biol. 244 (1994) 1–5.
[17] D. Snyder, J. Lary, Y.L. Chen, P. Gollnick, J.L. Cole, Interaction of the *trp* RNA-binding attenuation protein (TRAP) with anti-TRAP, J. Mol. Biol. 338 (2004) 669–682.
[18] A. Ruhe, P.A. Wedin, Algorithms for separable nonlinear least squares problems, SIAM Rev. 22 (1980) 318–336.
[19] P. Schuck, B. Demeler, Direct sedimentation analysis of interference optical data in analytical ultracentrifugation, Biophys. J. 76 (1999) 2288–2296.
[20] B. Efron, R. Tibshirani, Bootstrap methods for standard errors, confidence intervals, and other measures of statistical accuracy, Statist. Sci. 1 (1986) 54–77.
[21] P. Schuck, Some statistical properties of differencing schemes for baseline correction of sedimentation velocity data, Anal. Biochem. 401 (2010) 280–287.
[22] W.F. Stafford, P.J. Sherwood, Analysis of heterologous interacting systems by sedimentation velocity: curve fitting algorithms for estimation of sedimentation coefficients, equilibrium, and kinetic constants, Biophys. Chem. 108 (2004) 231–243.